Neurobiology of Disease 177 (2023) 105983

Contents lists available at ScienceDirect

Neurobiology of Disease

journal homepage: www.elsevier.com/locate/ynbdi

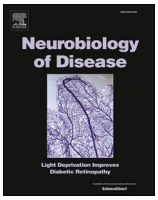

Regional transcriptional vulnerability to basal forebrain functional dysconnectivity in mild cognitive impairment patients

Peng Ren [a,b,1], Wencai Ding [c,1], Siyang Li [a,b], Guiyou Liu [d,e], Meng Luo [a], Wenyang Zhou [a], Rui Cheng [a], Yiqun Li [a], Pingping Wang [a], Zhipeng Li [a,b], Lifen Yao [c], Qinghua Jiang [a,f,*], Xia Liang [a,b,*], for the Alzheimer's Disease Neuroimaging Initiative[2]

[a] School of Life Science and Technology, Harbin Institute of Technology, Harbin 150001, China
[b] Laboratory for Space Environment and Physical Science, Harbin Institute of Technology, Harbin 150001, China
[c] Department of Neurology, First Affiliated Hospital of Harbin Medical University, Harbin 150001, China
[d] Beijing Institute for Brain Disorders, Laboratory of Brain Disorders, Ministry of Science and Technology, Collaborative Innovation Center for Brain Disorders, Capital Medical University, Beijing 100069, China
[e] Department of Neurology, Xuanwu Hospital, Capital Medical University, Beijing 100053, China
[f] Key Laboratory of Biological Big Data (Harbin Institute of Technology), Ministry of Education, Harbin 150001, China

ARTICLE INFO

Keywords:
Nucleus basalis of Meynert
Functional connectivity
Mild cognitive impairment
Basal forebrain
Transcriptional vulnerability
Tissue-specific geneset risk score

ABSTRACT

Nucleus basalis of Meynert (NbM), one of the earliest targets of Alzheimer's disease (AD), may act as a seed for pathological spreading to its connected regions. However, the underlying basis of regional vulnerability to NbM dysconnectivity remains unclear. NbM functional dysconnectivity was assessed using resting-state fMRI data of health controls and mild cognitive impairment (MCI) patients from the Alzheimer's disease Neuroimaging Initiative (ADNI2/GO phase). Transcriptional correlates of NbM dysconnectivity was explored by leveraging public intrinsic and differential post-mortem brain-wide gene expression datasets from Allen Human Brain Atlas (AHBA) and Mount Sinai Brain Bank (MSBB). By constructing an individual-level tissue-specific gene set risk score (TGRS), we evaluated the contribution of NbM dysconnectivity-correlated gene sets to change rate of cerebral spinal fluid (CSF) biomarkers during preclinical stage of AD, as well as to MCI onset age. An independent cohort of health controls and MCI patients from ADNI3 was used to validate our main findings. Between-group comparison revealed significant connectivity reduction between the right NbM and right middle temporal gyrus in MCI. This regional vulnerability to NbM dysconnectivity correlated with intrinsic expression of genes enriched in protein and immune functions, as well as with differential expression of genes enriched in cholinergic receptors, immune, vascular and energy metabolism functions. TGRS of these NbM dysconnectivity-correlated gene sets are associated with longitudinal amyloid-beta change at preclinical stages of AD, and contributed to MCI onset age independent of traditional AD risks. Our findings revealed the transcriptional vulnerability to NbM dysconnectivity and their crucial role in explaining preclinical amyloid-beta change and MCI onset age, which offer new insights into the early AD pathology and encourage more investigation and clinical trials targeting NbM.

1. Introduction

Cholinergic system degeneration is a primary pathogenetic event in Alzheimer's disease (AD). Recent histological and in vivo volumetric evidence suggests that the nucleus basalis of Meynert (NbM), a major source of cholinergic innervation to the cerebral cortex, exhibits

Abbreviations: NbM, nucleus basalis of Meynert; FC, functional connectivity; MCI, mild cognitive impairment; TGRS, tissue-specific geneset risk score.

* Corresponding authors at: Harbin Institute of Technology, Harbin, China.
E-mail addresses: qhjiang@hit.edu.cn (Q. Jiang), xia.liang@hit.edu.cn (X. Liang).

[1] These authors contributed equally to this work.

[2] Data used in preparation of this article were obtained from the Alzheimer's Disease Neuroimaging Initiative (ADNI) database (adni.loni.usc.edu). As such, the investigators within the ADNI contributed to the design and implementation of ADNI and/or provided data but did not participate in analysis or writing of this report. A complete listing of ADNI investigators can be found at: http://adni.loni.usc.edu/wp-content/uploads/how_to_apply/ADNI_Acknowledgement_List.pdf

https://doi.org/10.1016/j.nbd.2022.105983
Received 8 September 2022; Received in revised form 7 December 2022; Accepted 28 December 2022
Available online 29 December 2022

severely cholinergic neuron loss in AD and may start to degenerate from the very early phases of AD (Grothe et al., 2013; Schliebs and Arendt, 2011; Weigand et al., 2020; Xu et al., 2021).

As an early event in the course of AD, NbM degeneration may interact with other etiologic factors to facilitate spreading of AD pathology to the cortex. Cholinergic NbM atrophy in preclinical stages of AD measured in vivo on MRI is associated with amyloid pathology in widespread cholinergic innervated cortical areas (Kerbler et al., 2015; Teipel et al., 2014). In the course of AD, NbM atrophy is demonstrated to be a reliable upstream event of subsequent entorhinal and neocortical degeneration (Fernandez-Cabello et al., 2020; Schmitz et al., 2016). Furthermore, longitudinal degeneration of the cholinergic basal forebrain covaries with longitudinal degeneration of multiple cholinergic innervated cortical regions, and overlaps with PET indices of cholinergic denervation (Schmitz et al., 2018). Recent resting-state functional MRI (rsfMRI) studies show reduced NbM functional connectivity with cholinergic projected brain areas during early phases of AD (Li et al., 2017; Meng et al., 2018; Qi et al., 2021), and the functionally disconnected regions are not completely spatially overlapped with those structurally degenerated. Together, these evidences suggest that the spatial topography of dysregulated NbM-cortex interactions may reflect varied regional vulnerability to the interdependence between NbM deficiency and other AD pathologies that could not be captured by spreading of structural degeneration. However, it remains ambiguous what mechanisms may be involved in determining the spatial topography of NbM dysconnectivity at the early stages of AD.

Here we aimed to investigate the underlying determinants of the varied regional vulnerability to NbM functional dysconnectivity at the early stages of AD, by examining the transcriptomic correlates of the NbM dysconnectivity patterns in mild cognitive impairment (MCI) patients. NbM dysconnectivity pattern was explored using fMRI data from Alzheimer's Disease Neuroimaging Initiative (ADNI). To investigate whether the NbM dysconnectivity topography is associated with pre-existing transcriptional heterogeneity, or manifests as a sideshow of genetic aberrations that are unevenly distributed across the brain, we assessed both normative (Hawrylycz et al., 2015; Hawrylycz et al., 2012) and differential brain-wide transcriptional profiles (Haroutunian et al., 2009). These two sets of gene expression profiles were separately correlated with NbM dysconnectivity pattern, followed by Gene Set Enrichment Analysis (GSEA) to characterize the intrinsic or differential expression of genes involved in neurotransmitter systems, cell types and biological pathways. Finally, based on the identified gene sets underlying NbM dysconnectivity distribution, we constructed an individual-level tissue-specific gene set risk score, in attempt to evaluate their relation with preclinical longitudinal changes of CSF biomarkers and MCI onset age.

2. Material and methods

2.1. Participants

We selected 49 healthy controls (HC) and 62 clinical defined MCI participants (Table 1, detailed in Supplementary Table 1 and Supplementary Method) from phases GO/2 of the ADNI database (ADNI2/GO, https://adni.loni.usc.edu/). 56 participants being HC at baseline and later developed MCI during the visits (demographics in Supplementary Table 3) were selected from ADNI2/GO for regression analyses between genomic and clinical characteristics. Additional 104 HC and 44 MCI participants from phase 3 of the ADNI database (ADNI3) were used for validation. Study subjects gave written informed consent and the study was approved by each participating site's Institutional Review Board. Detailed information regarding recruitment and diagnostic criteria can be found on the ADNI website (www.adni-info.org).

Table 1
Demographic and clinical features of the participants.

	HC ($n = 49$)	MCI ($n = 62$)	*P*
Demographics			
Age, years	74.60 ±6.90	71.56± 7.98	0.033[a]
Sex (M/F)	16/33	32/30	0.055[c]
Education years	16.47±2.37	16.02±2.56	0.337[a]
Handedness (L/R)	6/43	3/59	0.180[c]
Clinical features			
MMSE	28.94±1.23	27.91±1.71	**<0.001**[b,d]
CDR	0.01±0.07	0.49±0.06	**<0.001**[a,e]
Delayed logical memory	14.03±2.86	6.11±3.27	**<0.001**[a,f]
Immediate logical memory	15.08±3.07	8.32±3.16	**<0.001**[a,f]

Average values are reported as mean ± SD and significant differences are highlighted in bold.
MCI = Mild cognitive impairment patients; HC = healthy controls; n = sample size; F = female; M = male; L = left; R = right; MMSE = Mini-Mental State Examination; CDR = Clinical Dementia Rating.
[a] significance checked with two-sided independent two sample Student's *t*-test.
[b] significance checked with two-sided independent two sample Welch's *t*-test.
[c] significance checked with Fisher's exact test.
[d] only available for 48 and 55 MCI participants.
[e] only available for 49 and 61 MCI participants.
[f] only available for 39 NC and 44 MCI participants.

2.2. MRI data preprocessing and seed-based functional connectivity

rsfMRI images from ADNI2/GO/3 were preprocessed using AFNI (version 21.2.04; https://afni.nimh.nih.gov/) with a standard processing pipeline (Supplement).

The seed regions of interest (ROIs) for bilateral NbM were defined using the SPM Anatomy toolbox (Eickhoff et al., 2005; Zaborszky et al., 2008), with a probability threshold of 0.6 (Fig. 1A). Pearson's correlation between the mean time course of each NbM seed and the time course of every voxel in the brain was calculated, followed by Fisher's r-to-z transformation. For each bilateral NbM ROI, the resultant resting state functional connectivity (rsFC) maps were submitted to a two-sample *t*-test between the MCI and HC group, masked by an *or* map of significant within-group NbM connectivity in each group (i.e., significant NbM rsFC in HC *or* MCI group). The significant within-group NbM rsFC map was thresholded under FWE-corrected $P < 0.05$ (one-sample t-test). The significant NbM rsFC map generated within the HC group was referred to as the normative NbM rsFC map from now on. The demographic variables (age, sex, and years of education), together with mean frame displacement, the number of remaining TRs after scrubbing and scanner effect were included as covariates. A significance threshold of family wise error rate (FWE)-corrected $P < 0.05$ was set for all rsFC analyses unless otherwise specified.

2.3. Gene expression dataset processing

Intrinsic regional transcriptional profiles were assessed using the whole brain microarray normal gene expression data provided by Allen Human Brain Atlas (AHBA; http://human.brain-map.org/) (Hawrylycz et al., 2015; Hawrylycz et al., 2012). A standard pipeline was used for processing (Arnatkeviciute et al., 2019). Only left-hemisphere samples were used for all analyses (Hawrylycz et al., 2015). Furthermore, we restricted our analyses to brain-expressed genes (15,655 genes) adapted from Human Protein Atlas (HPA; https://www.proteinatlas.org/) (Sjöstedt et al., 2020). A regional gene expression matrix of 246 regions × 15,655 genes was finally used for further analyses (see Supplemental eMethods).

MCI-related differential gene expression profiles were obtained from the Mount Sinai Brain Bank (MSBB; https://www.synapse.org/#!Synapse:syn16809559) study (see Supplemental eMethods), with

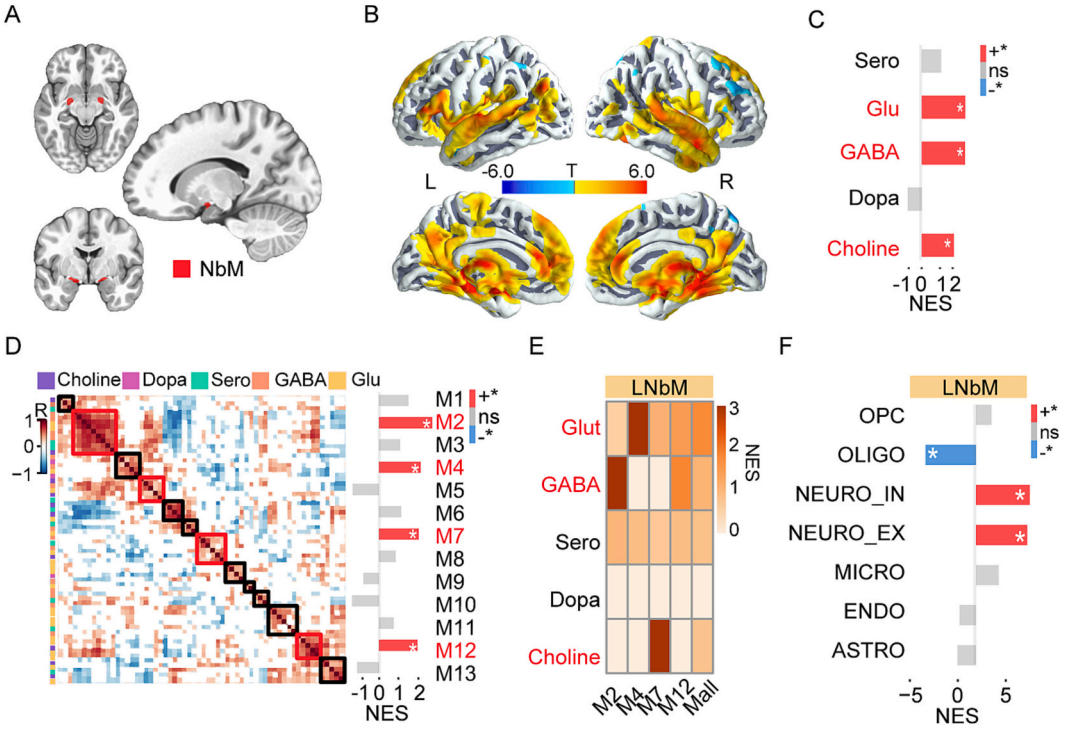

Fig. 1. Transcriptional profile underlying normative NbM rsFC. (A) Bilateral basal forebrain NbM seed regions in MNI space. **(B)** Distribution of significant LNbM rsFC in HCs. Subcortical areas are displayed in ventricular areas as approximations. **(C)** Neurotransmitter basis of LNbM rsFC revealed by GSEA enrichment of five neurotransmitter systems (cholinergic, dopaminergic, serotoninergic, GABAergic, and glutamatergic) **(D)** Neurotransmitter co-expression modules (left panel) enriched in LNbM connected areas (right panel). Receptor genes are labeled with different colors denoting their corresponding neurotransmitter system. Significantly enriched modules are also shown with red squares in the left panel. **(E)** The significantly enriched neurotransmitter modules correlating with LNbM rsFC patterns are dominated by glutamatergic, GABAergic and cholinergic receptors. **(F)** Cellular basis of normal LNbM rsFC identified by cell-type enrichment analysis. Significantly positively (red) and negatively (blue) enriched cell types are shown. * $P_{FDR} < 0.05$. MNI, Montreal Neurological Institute; LNbM, left NbM; rsFC, resting state function connectivity; HCs, healthy controls; Choline, cholinergic; Dopa, dopaminergic; Sero, serotoninergic; GABA, GABAergic; Glu, glutamatergic; Astro, astrocyte; Micro, microglia; OPC, oligodendrocyte precursor; Oligo, oligodendrocyte; Endo, endothelial; Neuro-ex, excitatory neurons; Neuro-in, inhibitory neurons; M, module; Mall, all the enriched modules for the corresponding case and hemisphere; ns, non- significant; GSEA, gene set enrichment analysis; NES, normalized effect size. (For interpretation of the references to colour in this figure legend, the reader is referred to the web version of this article.)

microarray probes assayed from 19 AD-related brain regions (left hemisphere) (Haroutunian et al., 2009; Hodes and Buckholtz, 2016; Wang et al., 2016). We used the common gene set (14,283 genes) assayed by MSBB and AHBA for further analysis. Differential gene expression between the HC and MCI samples was computed with limma R package. No *P* threshold was applied since we are interested in the entire gene list.

2.4. Neurotransmitter, cellular and biological enrichment analysis

To investigate the transcriptional basis of the NbM rsFC pattern, we calculated the Spearman correlations between the normative NbM rsFC map and intrinsic gene expression map. We also compared the NbM functional dysconnectivity pattern with the intrinsic gene expression map and the MCI-related differential gene expression profile. Each resulting correlation list was ranked in descending order and fed into gene set enrichment analyses to determine whether NbM ROIs tend to connect or dysconnect with brain regions enriched with genes associated with specific neurotransmitter, cellular or biological processes.

To investigate the neurotransmitter basis underlying NbM rsFC and its MCI-related alteration pattern, 60 neurotransmitter receptor genes from five main neurotransmitter systems (serotonergic, glutamatergic, cholinergic, dopaminergic and GABAergic) were selected from the corresponding Kyoto Encyclopedia of Genes and Genomes (KEGG) (Kanehisa and Goto, 2000) pathways (Supplementary Table 2). We examined the enrichment of the five neurotransmitter systems in each ranked gene list using customized GSEA (Subramanian et al., 2005). For the NbM rsFC pattern, an extra enrichment analysis across neurotransmitter co-expression networks was conducted (see Supplemental Methods). All GSEA were performed using GSEA-P 4.1.0 (Subramanian et al., 2005).

We obtained cell type-specific gene sets for seven cell types from a prior study (Seidlitz et al., 2020). The seven classes were: astrocytes, endothelial cells, microglia, excitatory neurons, inhibitory neurons, oligodendrocytes, and oligodendrocyte progenitor cells. GSEA was conducted for each ranked gene list to test the enrichment of the seven cell types.

The more general involvement of the biological basis was characterized by Gene Ontology (GO) biological processes and KEGG pathways. Enrichment of these processes/pathways in each ranked gene list was conducted using the GAGE method (Luo et al., 2009) in gage R package. The relationship between the enrichment results was further qualitatively explored with chord diagram.

A false discovery rate (FDR) corrected $P_{FDR} < 0.05$ was set for GO/KEGG and neurotransmitter enrichment analysis, while a $P_{FDR} < 0.001$ and normalized effect size (NES) > 4 were applied to the cellular enrichment analysis.

2.5. Construction of gene set specific risk score

For each identified gene set from the above analysis, we extracted its gene co-expression subnetwork based on the hippocampus-specific co-expression network from Genotype-Tissue Expression (GTEx) Portal ($P_{FDR} < 0.05$). Independent significant expression quantitative trait loci (eQTLs) for autosomal chromosomes, which measure the regulatory

effect of single-nucleotide polymorphisms (SNPs) on gene expression, were extracted for genes in each identified gene set. For each subject, Tissue-specific Gene set Risk Score (TGRS) was defined by combining the co-expression sub-network and individual genomic profile with eQTLs (Fig. 4A):

$$\mathrm{TGRS}(P) = \sum_{i=1}^{G}\left(D_i \sum_{i,j=1}^{V}\beta_{i,j}N_j\right) \quad (1)$$

Here, P is the gene set of interest with a total of G genes and V is the number of independent SNPs for the ith gene. D_i is the sum of the strengths of the directly connected edges of the ith gene, while $\beta_{i,\,j}$ denotes the normalized eQTL effect size of the jth SNP on the expression of the ith gene and N_j is the genotype of the jth SNP for a given participant.

Individual genotypes for MCI subjects from ADNI2/GO were processed with recommended quality control steps (Marees et al., 2018). The 1000 Genome phase 3 release (Altshuler et al., 2015) for the European population was used to characterize the linkage disequilibrium (LD) of SNPs (see details in Supplementary methods).

TGRSs were computed for each of the enriched neurotransmitter, cellular and biological pathway gene sets. Given the large number of biological pathway enriched gene sets, their corresponding TGRS scores were first dimensionally reduced using principal component analysis (PCA). For across-stages prediction, PCA was conducted across HC participants converted to MCI (pre-diagnosis) and those MCI patients diagnosed at baseline (post-diagnosis), while for the prediction in separate stages, the PCA were conducted in participants in the corresponding stages. The first 10 PCs were selected and then rotated with varimax method before further analysis. PCA was performed with R package "stats".

2.6. Relationship between TGRS and annual change rate of CSF biomarkers

In exploring the relationship of the proposed risk score to early pathology, we tested whether the TGRSs of NbM dysconnectivity transcriptional correlates contribute to longitudinal change rate of three CSF biomarkers: amyloid beta 42 (Aβ42), amyloid beta 42/40 (Aβ42/40) and tau phosphorylated at threonine 181 (ptau). The change rate of CSF biomarkers was calculated using linear mixed effect model, with month of sampling, age at baseline, gender and baseline CSF biomarkers as fixed effect. Additionally, random intercept and random slope in month were also included. The change rate of CSF biomarkers were estimated before MCI diagnosis (in 56 MCI patients with available pre-diagnosis data) and after MCI diagnosis, respectively.

As previous work has revealed that polygenetic risk score was associated with brain regional volume in healthy controls but not Alzheimer's disease patients (Wang et al., 2019), we wonder if the proposed TGRSs score would contribute more at pre-diagnosis stage. The prediction analysis was conducted in MCI patients across pre-diagnosis and post-diagnosis stages, and in each separate stage, respectively. The first 10 principal components of biological processes TGRSs, as well as TGRSs for cell types and neurotransmitters were separately entered into stepwise regressions to select possible explanatory variables for change rate of biomarkers. The bidirectional stepwise regression from R package "olsrr" was used. Age at baseline and gender were forced included in the model, the education year, *APOE* ε4 genotype and polygenic hazard score (PHS) from prior work (Desikan et al., 2017) were included as candidate variables in the regressions. At each step, variables were added based on $P < 0.05$, and the AIC was used to set a limit on the total number of variables included in the final model. To explain the function of each discovered varimax-rotated component (VC), we ranked the contributors to the component by absolute loadings and the processes/pathways with loading >0.5 were considered the primary functions of the component.

2.7. Relationship between TGRS and MCI onset age

In further exploring the potential contribution of the proposed risk score to early MCI pathology, we tested whether the TGRSs of the NbM dysconnectivity transcriptional correlates contributed to MCI onset age. We used age at MCI conversion visit of HC as an approximate MCI onset age. The same stepwise regression analyses and interpretations were conducted as change of biomarkers in pre-diagnosis MCI group.

2.8. Validation analyses

We validated our main findings by repeating the analyses on ADNI3. The regression analysis with MCI onset age and change of biomarkers were not performed on ADNI3 due to insufficient number of MCI subjects with pre-diagnosis data.

3. Results

3.1. Transcriptomic correlates of normative NbM rsFC

In HC group, both the left and right NbM displayed extensive positive rsFC to the surrounding subcortical structures in hippocampus, amygdala, putamen, caudate, and thalamus, as well as to cortical areas in the medial prefrontal/anterior cingulate cortex, posterior cingulate cortex/precuneus, insular and middle temporal cortices (Fig. 1B and Supplementary Fig. 1B).

Spatial correlations between NbM rsFC pattern and intrinsic regional gene expression profiles revealed significant positive enrichment of cholinergic, glutamatergic and GABAergic receptor genes (Fig. 1C and Supplementary Fig. 1C). We further evaluated the spatial co-expression between 60 neurotransmitter receptor genes across the NbM-connected regions (Supplementary Fig. 3). Each of the co-expression module consisted of genes from multiple neurotransmitter systems (Fig. 1D, Fig. 2 and Supplementary Fig. 1D). Genes associated with the NbM rsFC pattern were enriched in multiple neurotransmitter modules (Fig. 1D and Supplementary Fig. 1D), which were mainly involved in glutamatergic and GABAergic systems while a few of them appeared to be involved in the cholinergic system (Fig. 1E and Supplementary Fig. 1E). For validation, the enriched modules (Supplementary Fig. 2B—C) of co-expression network built across the whole brain (Supplementary Fig. 2A) showed a significant overlap with those for the left ($P = 0.030$; Supplementary Fig. 2D) and right NbM ($P < 0.001$; Supplementary Fig. 2E) connected regions. Similar neurotransmitter involvement was found for these modules (Supplementary Fig. 2F).

We also evaluated whether genes spatially related to NbM connectivity were enriched in certain cell types. GSEA results revealed significant positive enrichment of excitatory and inhibitory neurons and negative enrichment of oligodendrocytes in brain regions with high NbM rsFC (FDR-corrected $P < 0.001$ and $NES > 4$; Fig. 1F and Supplementary Fig. 1F).

3.2. Functional dysconnectivity of the NbM in MCI patients

Comparisons in NbM rsFC between MCI and HC revealed apparent varied changes of NbM rsFC across different brain regions (Fig. 3A-B). For left NbM, We found marginally significant rsFC decrease in left inferior frontal gyrus (uncorrected $P < 0.05$, Fig. 3C). For right NbM, we found significant rsFC decrease in the right middle temporal gyrus (FWE corrected $P < 0.05$), together with marginally significant rsFC decrease in left middle temporal and superior frontal gyrus (uncorrected $P < 0.05$, Fig. 3C). NbM rsFC was also significantly correlated with Mini-Mental State Examination (MMSE) and delayed logical memory test (LDEL) in MCI patients (Supplementary Fig. 4).

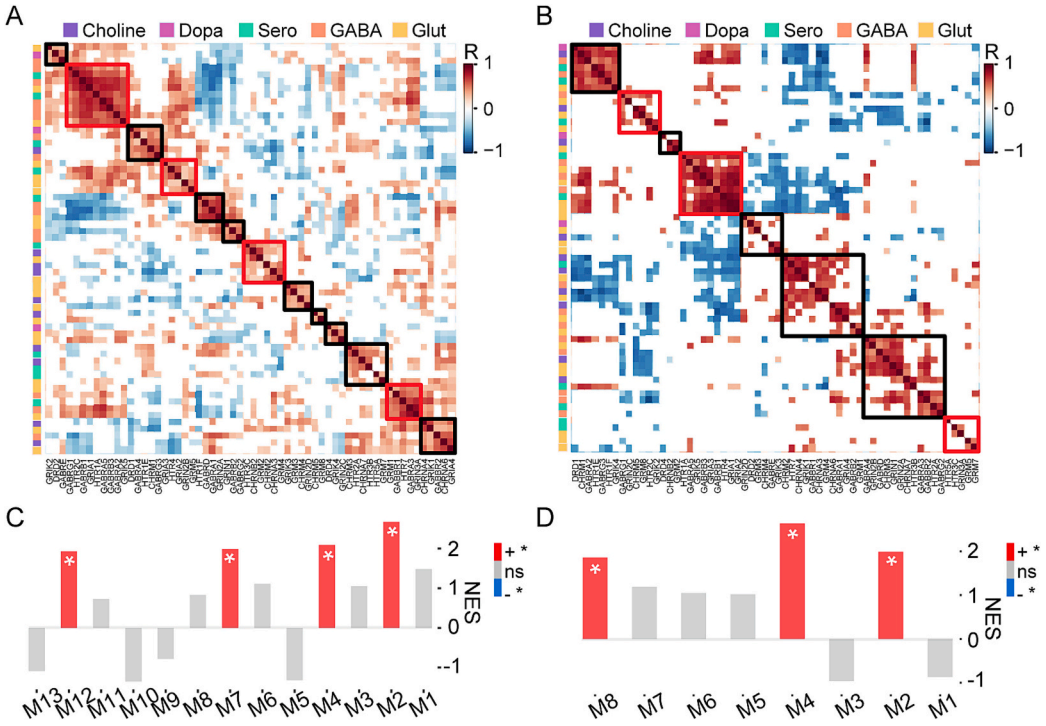

Fig. 2. Co-expression pattern details for the neurotransmitter receptors in areas with significant NbM FC. Co-expression pattern for the cholinergic, dopaminergic, serotoninergic, GABAergic, glutamatergic neurotransmitter receptors in the areas with significant LNbM **(A)** or RNbM **(B)** FC was demonstrated. The complete linkage was used to identify the clusters (all squares) and the insignificant correlations are showed in blank. Receptors of neurotransmitter systems are labeled with corresponding colors. Neurotransmitter basis underlying normal LNbM **(C)** or RNbM **(D)** FC was revealed by GSEA enrichment of the ranked gene list across modules in A and B, the list was derived by Spearman's correlation of LNbM or RNbM FC with Allen Human Brain Atlas transcriptional profile. Only significantly positively (red) enriched modules were discovered, which are also shown with red squares in (A, B). * denotes FDR corrected $P < 0.05$. LNbM, left NbM; RNbM, right NbM; Choline, cholinergic; Dopa, dopaminergic; Sero, serotoninergic; GABA, GABAergic; Glu, glutatmatergic; ns, non-significant; M, module; NES, normalized effect size; ns, non-significant. (For interpretation of the references to colour in this figure legend, the reader is referred to the web version of this article.)

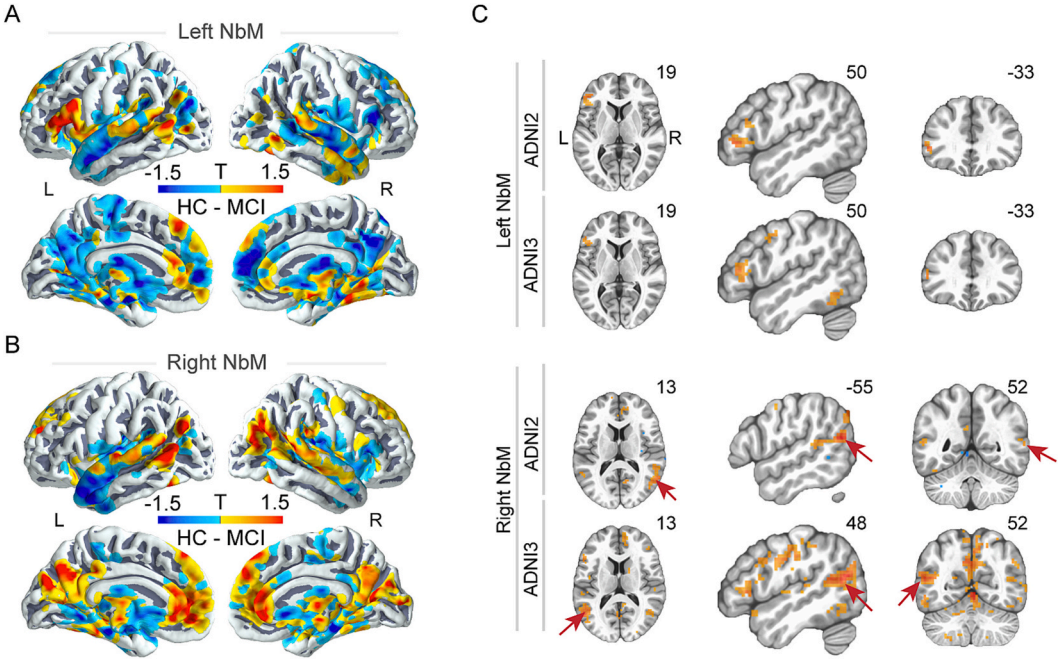

Fig. 3. The NbM functional dysconnectivity in MCI. LNbM **(A)** and RNbM **(B)** functional dysconnectivity patterns in MCI patients are shown in surface space. Warm colors represent decreased rsFC and cold colors represent increased rsFC in patients with MCI. **(C)** For LNbM, between group comparisons revealed marginally significant rsFC reduction in the left inferior frontal gyrus (top panel). While for RNbM, significant reduction in the right middle temporal gyrus, as well as marginally significant reduction in the superior frontal gyrus and left middle temporal gyrus were found (bottom panel). Similar clusters were observed in validation analysis on ADNI3. The clusters are thresholded at voxel-wise $P < 0.05$ and cluster size >40, the red arrow indicates clusters significant at FWE corrected $P < 0.05$. LNbM, left NbM; RNbM, right NbM. (For interpretation of the references to colour in this figure legend, the reader is referred to the web version of this article.)

3.3. Transcriptional correlates of NbM functional dysconnectivity in MCI

To investigate the putative pre-existing transcriptional properties underlying differential regional vulnerability to NbM dysconnectivity in MCI, we evaluated spatial correlations between NbM rsFC changes in MCI and intrinsic regional gene expression profiles. We observed no significant enrichment in neurotransmitter system for genes related to NbM dysconnectivity pattern (Figure 4Ai-ii, left panel). Brain regions with higher vulnerability to NbM rsFC alteration in MCI were positively enriched with genes related to excitatory neurons and negatively enriched with genes in microglia and astrocyte cell types (Figure 4Bi-ii, left panel). Moreover, for the left NbM, vulnerable brain regions were enriched with gene sets associated with different aspects of protein translation, while for the right NbM, the enriched gene sets were related to protein translation, as well as immune functions including leukocyte and granulocyte activation (Fig. 4C). We denoted these enrichment results by correlating with intrinsic gene expressions as risk gene sets.

We also correlated the NbM rsFC alteration pattern in MCI with MCI-specific gene differential expression (DE) profiles. GSEA revealed the cholinergic receptor genes to be positively enriched in brain regions dysconnected with the NbM (Figure 4Ai-ii, right panel). Moreover, we found gene sets implicated in microglia, astrocytes and endothelia cells to be positively enriched, while gene sets of excitatory and inhibitory neurons to be negatively enriched in NbM disconnected regions (Figure 4Bi-ii, right panel). Enrichment analysis of biological pathways/processes revealed positively enriched gene sets related to blood vessel development and negatively enriched gene sets related to multiple aspects of energy metabolism, including ATP synthesis and mitochondrion functions (Fig. 4C). We referred to the above enrichment results obtained from the differential expressed gene maps as DE gene sets.

To explore the potential relationship between risk and DE gene sets, we examined their intersection and found almost no common enriched gene sets of intrinsic and DE map for bilateral NbM (Fig. 4C, right panel).

3.4. NbM dysconnectivity associated gene sets contribute to preclinical longitudinal change of CSF biomarkers

Having identified the enriched gene sets for vulnerable NbM connectivity to MCI, we next investigated whether these gene sets were associated with early pathological changes. Group-level identified gene sets were translated to individual-level genetic risk score (TGRS, Fig. 5A). As for each patient, the proposed TGRS are genetic risk scores that keep constant across healthy and different disease stages, it would be reasonable to speculate that the TGRS plays different roles in different stages. Specifically, TGRS may play a potential risk role in healthy stage of patients that drive the pathological changes and the onset of the clinical symptoms. To test this hypothesis, we first regressed TGRS against change rate of CSF biomarkers in all MCI patients and found no significant predictors of longitudinal change of CSF biomarkers. We thus further conducted regression analysis before and after MCI diagnosis, respectively (Fig. 5B). Our results revealed significant predictors in explaining pre-diagnosis rather than post-diagnosis longitudinal changes in CSF biomarkers. Specifically, at the pre-diagnosis stage, starting from the top 10 varimax-rotated components of GSEA enriched biological processes as input variables, the step-wise regression analysis identified two component (VC3, VC4), which mainly contained gene sets implicated in vascular and immune functions, as predictors for change rate of Aβ42/40 (Fig. 5C and Table 2). In contrast, at the post-diagnosis stage, no significant predictors were selected for longitudinal change of CSF biomarkers (Table 2). Moreover, using TGRS of cellular and cholinergic enriched gene sets as input variables, no significant predictors were selected by step-wise regressions (Supplementary Table 4).

3.5. NbM dysconnectivity associated gene sets contribute to MCI onset age

The MCI onset age is a unique clinical milestone and can only be obtained by longitudinal visits of normal subjects at risk. Within the 56 MCI patients with available pre-diagnosis data, MCI onset age can be accurately assessed, allowing us to investigate whether the gene sets at risk for NbM dysconnectivity were associated with the age of MCI onset. With the top 10 principal components of GSEA enriched biological processes as input variables, the step-wise regression analysis selected two components (VC3 and VC8) as predictors for MCI onset age (Fig. 5D, Table 2). VC3 mainly contained genes sets implicated in immune function, while gene sets within VC8 were involved in various development processes (Fig. 5D). However, using TGRS of cellular and cholinergic enriched gene sets as input variables, no significant predictors were selected by step-wise regressions (Supplementary Table 4).

3.6. Validation analyses

To test the reliability of our findings, NbM functional connectivity and dysconnectivity maps, as well as their transcriptional correlates were validated using a separate cohort from ADNI3 (demographics in Supplementary Table 5), which yielded consistent results to our main analyses on ADNI2/GO. Specifically, we observed largely similar distribution of the normative NbM rsFC (Supplementary Fig. 5A-B), which was closely related to intrinsic gene expression enriched in cholinergic receptors and neuronal cell types (Supplementary Fig. 5C–D). Between-group comparisons revealed similar alteration patterns for both left and right NbM rsFC in ADNI3 (Fig. 3). Moreover, as in ADNI2/GO, the regions vulnerable to the NbM dysconnectivity were associated with the intrinsic expression of genes enriched in protein and immune functions, as well as with differential expression of genes enriched in cholinergic receptors, immune cells, blood vessel development (Supplementary Fig. 6).

4. Discussion

In this study, we first demonstrated the cholinergic and neuronal basis of normal NbM rsFC. We then explored the driving and driven transcriptional profiles underlying NbM dysconnectivity in MCI. We found that areas with high intrinsic expression in protein and immune function, and differential expression in cholinergic and energy metabolism were especially vulnerable to NbM rsFC alteration. Next, the discovered group-level gene sets were translated to individual risks, which were related to MCI onset age and longitudinal changes of CSF biomarkers in pre-diagnosis MCI, independent of traditional AD risks. Finally, the main findings on ADNI2/GO were recaptured on ADNI3 dataset. These findings provide insights in understanding the roles of NbM in the early AD pathology.

4.1. Neurotransmitter and cellular origins of baseline NbM functional connectivity map

Early studies established the NbM as the major cholinergic nucleus that sends projections to the neocortex and amygdala (Do et al., 2016; Woolf, 1991). Estimating temporal correlations based on resting-state fMRI signal, we confirmed the broad distribution of rsFC in the amygdala and neocortical areas with the NbM. More importantly, the NbM FC map was closely related to the spatial distribution of cholinergic, glutamatergic and GABAergic receptors. The identified cholinergic involvement provides the first evidence to demonstrate the cholinergic attribution to the fMRI-derived FC map of the NbM (Meng et al., 2018). The involvement of the major excitatory and inhibitory neurotransmitter systems underlying NbM connectivity may be explained by the intrinsic interactions between cholinergic and these two neurotransmitter systems (Grilli et al., 2009; Guo et al., 2012; Witten et al., 2010).

For cellular mechanisms, we discovered the bilateral NbM rsFCs

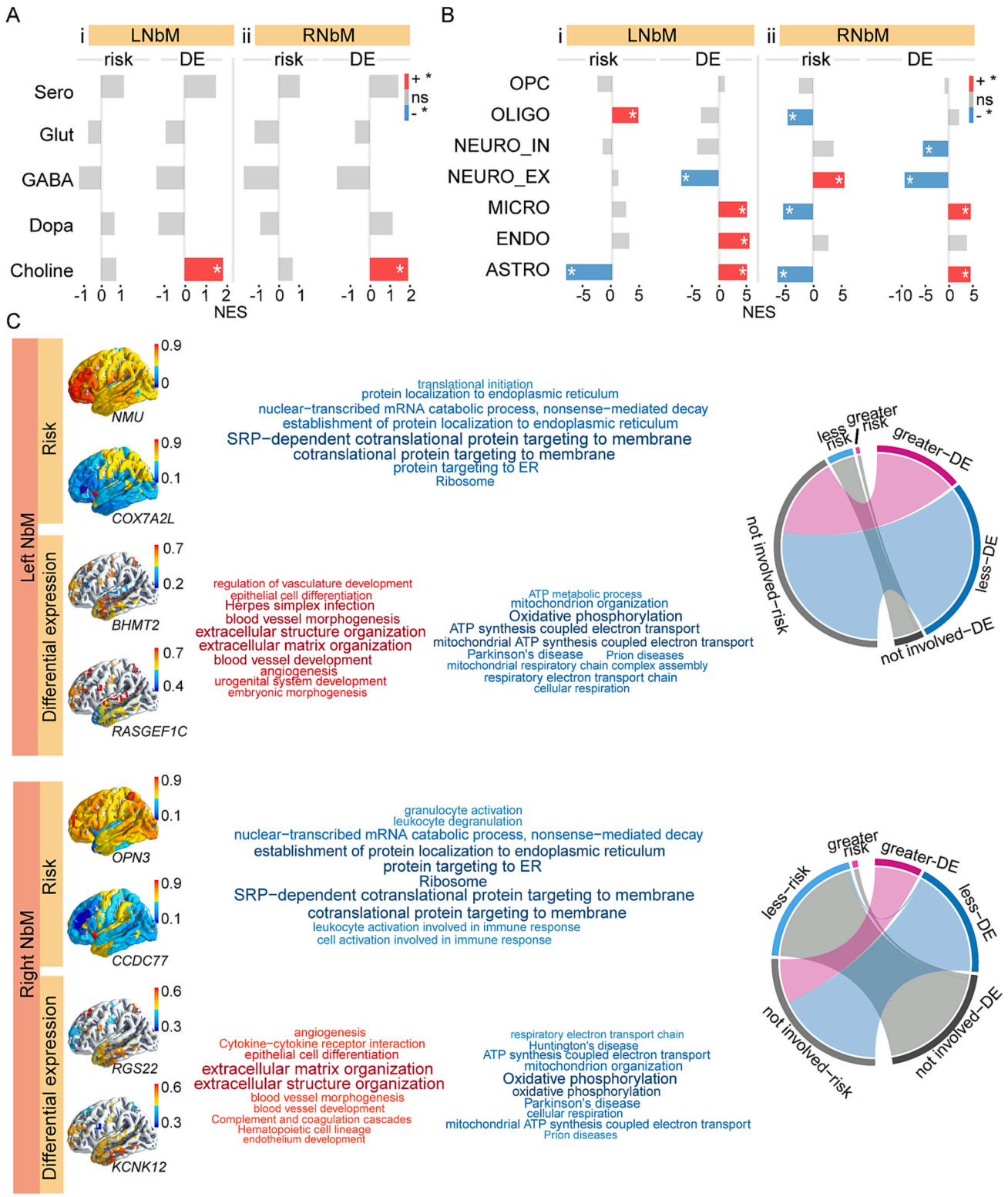

Fig. 4. Transcriptional basis underlying NbM rsFC alterations. GSEA enrichment of five neurotransmitter systems **(A)** and seven cell types **(B)** for genes related with NbM rsFC changes in MCI. **(C)** GAGE enrichment of GO biological processes and KEGG pathways for genes related with NbM rsFC changes in MCI. The brain expression pattern of the most positively or negatively correlated gene with normal or differential expression is shown (left panel). Top 10 positively (red) and negatively (blue) enriched pathways/processes are shown in the middle panel. Word size represents the degree of enrichment. The relationship between risk and DE processes/pathways is presented for LNbM or RNbM separately (right panel). * $P_{FDR} < 0.05$. LNbM, left NbM; RNbM, right NbM; GO, Gene Ontology; KEGG, Kyoto Encyclopedia of Genes and Genomes; DE, differential expression; Choline, cholinergic; Dopa, dopaminergic; Sero, serotoninergic; GABA, GABAergic; Glu, glutamatergic; Astro, astrocyte; Micro, microglia; OPC, oligodendrocyte precursor; Oligo, oligodendrocyte; Endo, endothelial; Neuro-ex, excitatory neurons; Neuro-in, inhibitory neurons; NES, normalized effect size; ns, non-significant. (For interpretation of the references to colour in this figure legend, the reader is referred to the web version of this article.)

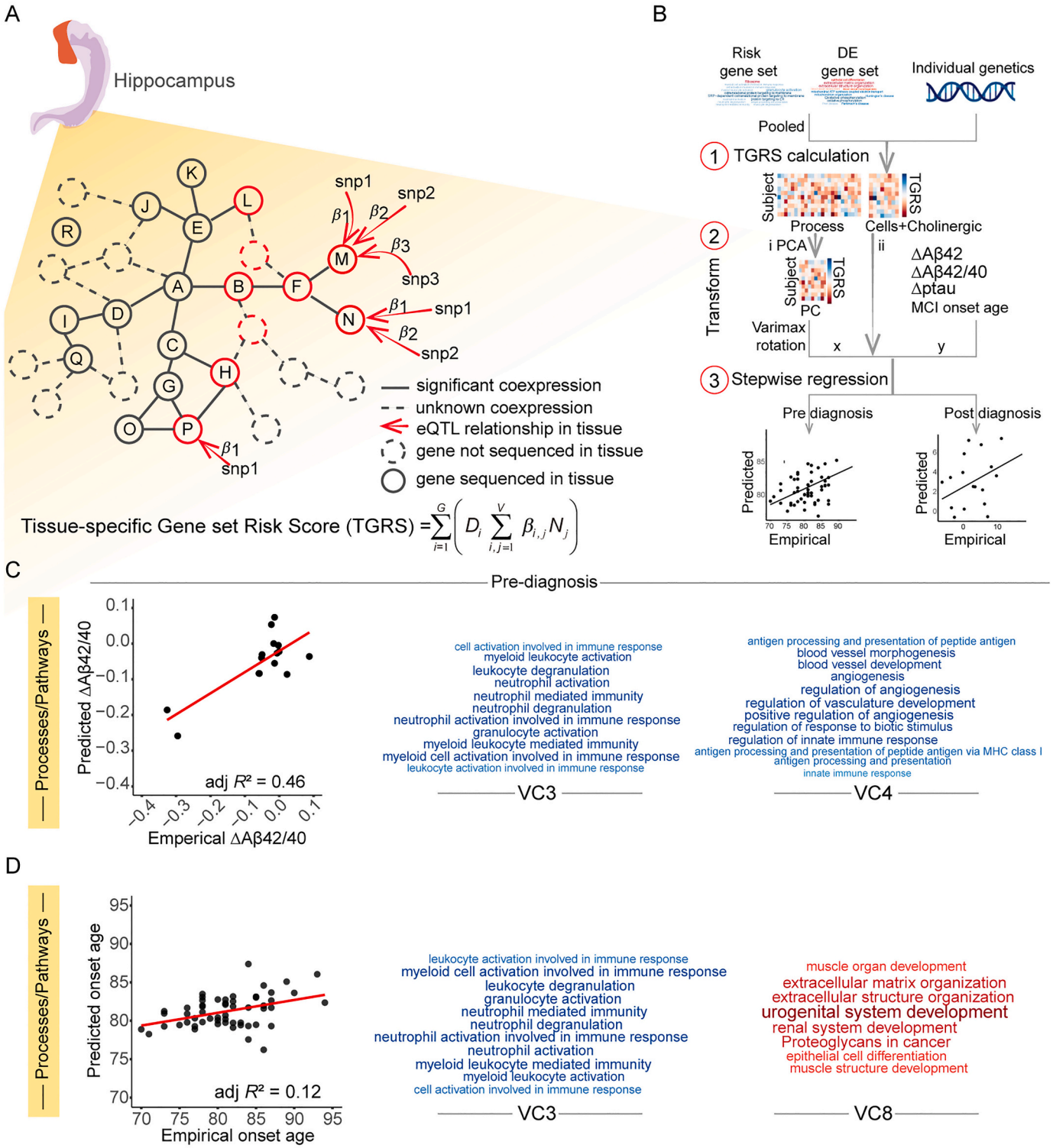

Fig. 5. Contribution of TGRS in explaining change rate of biomarkers and MCI onset age. (A) For each participant and gene set, a Tissue-specific Gene set Risk Score (TGRS) was constructed by integrating tissue-specific gene co-expression and individual genomics through SNP regulation of gene expression. Red circles represent the genes of a certain gene set. **(B)** Schematic of the regression analyses. **(C)** Scatter plots of predicted versus empirical outcome in pre-diagnosis MCI for significant regressions using VCs of pathways/processes TGRS as predictors. The pathways/processes with an absolute loading >0.5 are shown. Positive and negative contributors are shown in red and blue. Larger word size represents a greater degree of contribution to the corresponding TGRS varimax-rotated component. **(D)** Scatter plots of predicted versus empirical onset age in pre-diagnosis MCI for significant regressions using VCs of pathways/processes TGRS as predictors. The pathways/processes with an absolute loading >0.5 are shown. The colour and size are shown in the same way as (C). SNP/snp, single-nucleotide polymorphism; eQTL, expression quantitative trait loci; HC, health control; MCI, mild cognitive impairment; DE, differential expression; PCA, principal component analysis; VC, varimax-rotated component. (For interpretation of the references to colour in this figure legend, the reader is referred to the web version of this article.)

Table 2
Summary of stepwise regressions based on pathways/processes TGRS.

	ΔAβ42	*ΔAβ42/40*	*Δptau*	Onset age
Across stages				
	R^2 = 0.01,*P* = 0.269	R^2 = -0.01, *P* = 0.681	R^2 = 0.00, *P* = 0.418	
	PHS	–	–	
Separate stages				
Pre-diagnosis	R^2 = 0.11, *P* = 0.232	**R^2 = 0.46, *P* = 0.020**	R^2 = 0.00, *P* = 0.420	**R^2 = *0.12*, *P* = *0.022***
	VC4	VC3, VC4	–	VC3, VC8
Post-diagnosis	R^2 = 0.00, *P* = 0.376	R^2 = -0.01, *P* = 0.487	R^2 = 0.01, *P* = 0.246	
	–	–	Education	

Adjusted R^2 and predictors of final stepwise regression models are reported. The significant regressions are highlighted in bold.
TGRS = tissue-specific gene set risk score; ptau = tau phosphorylated at threonine 181; PHS = polygenetic hazard score; VC = varimax-rotated component.

were positively correlated with the distribution of excitatory and inhibitory neurons and negatively correlated with the distribution of oligodendrocytes and endothelial cells. These observations are partly consistent with previous evidence demonstrating that: (i) blood oxygenation level dependent (BOLD) signals reflect a mixture of astrocyte, excitatory and inhibitory neuronal activity (Fields et al., 2015; Lu et al., 2019; Moon et al., 2021) and (ii) oligodendrocytes and endothelial cells could modulate functional connectivity through genetic and physical regulation (Asleh et al., 2020; Kawamura et al., 2020; Meng et al., 2019). These findings, indicate an important role of both neuronal and non-neuronal cells underlying NbM rsFC and encourage further investigations.

4.2. NbM functional dysconnectivity in MCI patients

We found the right middle temporal gyrus exhibited significant reduced rsFC with the right NbM, and right superior frontal/right anterior cingulate tended to show reduced rsFC with the right NbM. These patterns are largely recaptured in validation analyses with ADNI3. This right NbM specific alteration pattern supports previous report that MCI group showed reduced anterior-NbM connectivity with the right superior medial frontal gyrus and reduced posterior-NbM connectivity with the right superior temporal area (Herdick et al., 2020). We anticipate that the investigation of the asymmetry feature of the NbM subregional rsFC alteration will further our understanding of the cholinergic role in the disease.

Moreover, alteration of the middle temporal gyrus, the key structure of the default mode network (DMN), is also supported by findings that FDG-PET hypometabolism in the inferior and middle temporal regions was a typical feature of subject cognitive complaint preclinical stage (Dong et al., 2021) and a robust predictor of the time of conversion to AD (Santangelo et al., 2020), These evidence, together with our findings, implies the early involvement of the middle temporal gyrus in MCI pathology.

4.3. Neurotransmitter, cellular, and genetic substrates underlying NbM connectivity vulnerability in MCI

We compared the spatial topography of NbM FC changes in MCI with both intrinsic and differential gene expression to understand the driving and driven transcriptomic correlates of NbM connectivity vulnerability. Enrichment analysis for neurotransmitter systems revealed that the differential but not intrinsic expression profile of gene sets related to NbM dysconnectivity were enriched in cholinergic receptors, the neurotransmitter system critically involved in NbM circuit activity. This finding recaptures recent studies reporting that donepezil therapy promoting cholinergic functions could increase the functional connectivity of the hippocampus in MCI (Pa et al., 2013), and provides novel evidence suggesting that the cholinergic signaling contributes to NbM dysconnectivity in MCI probably as a driven pathology, rather than a driving factor.

Another intriguing finding was that brain regions dysconnected with NbM in MCI were enriched with the normative expression of genes implicated in immune functions, including cell types of astrocytes and microglia, as well as biological processes such as myeloid leukocyte activation. These results align well with the well-known role of neuroinflammation and immune responses in the etiopathogenesis of AD (Wightman et al., 2021). Previous work provided evidence showing impaired anti-inflammation regulation in forebrain cholinergic neurons in AD (Lehner et al., 2019; Schmitz et al., 2020), and this impairment, indexed by basal forebrain volume loss, interacts with biomarkers of inflammation in preclinical group with abnormal amyloid and tau pathology (Schmitz et al., 2020). Our findings complement these earlier proofs by establishing that NbM dysconnectivity, an early phenotype of AD pathology, is more likely to target brain regions that are intrinsically enriched with astrocytes/microglia cells and/or immune process-related genes. Additionally, the MCI-specific DE of genes related to NbM dysconnectivity was enriched in astrocytes/microglia cells, indicating a crucial role of these cell types not only as a potential risk but also a key contributing factor as the disease progresses.

Finally, in brain regions vulnerable to NbM dysconnectivity, we found the enrichment of biological processes coordinating blood vessel development and energy metabolism in genes differentially expressed in MCI patients. This observation is in concordance with numerous studies demonstrating a close relationship between functional communications and metabolic demands in both healthy and degenerated brains (Liang et al., 2013; Marchitelli et al., 2018). Moreover, this corroborates with evidence suggesting that functional cholinergic system plays crucial role for the control of cerebral blood flow (Román and Kalaria, 2006).

4.4. Transcriptional genetic risks for NbM dysconnectivity contribute to MCI onset age and change of amyloid-beta pathology

Most existing research on dementia risk prediction typically evaluates individual-level genetic risk score (GRS) using variants identified by genome-wide association studies (GWAS) (Zhou et al., 2021). Given that most GWAS SNPs are regulatory and transcript characteristics are in a sense closer to the phenotype (Marigorta et al., 2017), recent work has demonstrated that transcriptional risk score (TRS) could provide an alternative estimate of disease risk to classical GRS. Our proposed framework provides an opportunity to translate population-level transcriptional risk to individual-level genetic risk through tissue-specific eQTL information. We found that the novel-defined TGRS based on transcriptional correlates of MCI-related NbM dysconnectivity can better explain change rate of CSF biomarkers in MCI during pre-diagnosis than post-diagnosis phases, which re-emphasizes the importance of NbM in the early pathology of MCI. Interestingly, the vascular and immune processes TGRS contributed positively to change rate of Aβ42/40 and MCI onset age. These findings indicate that the genetic profiles of these specific biological processes underlying NbM dysconnectivity may play a non-trivial role in promoting AD pathology at preclinical stages. The immune and vascular processes, may represent key endogenous pathways that closely interact with basal forebrain degeneration to contribute to early longitudinal changes of amyloid pathology (Nizari et al., 2021; Roher et al., 2000). Previous work has validated the PHS using GWAS can strongly predicted empirical AD onset age and decreased CSF Aβ42 (Desikan et al., 2017). Our results further implies that the TGRS of transcriptional correlates of NbM dysconnectivity can play an important role, beyond PHS and APOE, in explaining earlier traits such as MCI onset age and change of preclinical biomarkers. These results imply that the choice of the early neuroimaging biomarker of MCI, NbM rsFC, together with the combination of transcriptional

vulnerability model and TGRS, can reveal novel pathways and explaining individual risks independent of the traditional AD risks.

4.5. Limitations and future research

Several issues should be considered when interpreting our results. First, the bilateral NbM rsFC alteration patterns characterized on ADNI2/GO was only replicated at a less stringent threshold on ADNI3. The lack of robust rsFC difference between HC and MCI under FWE-corrected P threshold replicates an earlier finding from independent cohorts (Herdick et al., 2020). This may result in not robustly correlated biological functions in subsequent transcriptional correlation analysis. Future studies using a larger cohort for characterizing NbM rsFC alteration are required to further validate our findings. Second, the cellular, neurotransmitter, and biological enrichment analyses for bilateral NbM were performed only on the left hemisphere, preventing a comprehensive exploring of potential transcriptional differences underlying bilateral NbM rsFC and its alterations. Third, the DE profiles covered only AD related regions. This limited sampling strategy may have precluded the discovery of accurate DE profiles underlying NbM FC alteration. Fourth, the proposed TGRS of discovered gene sets related to MCI onset age and pre-diagnosis changes of CSF biomarkers, but given the limited sample of pre-diagnosed MCI in ADNI dataset, future studies with longitudinal follow-up on more normal subjects at risk are in warrant to gain more predictive power.

5. Conclusions

Our research provides a new framework for exploring the transcriptional characteristics underlying functional dysconnectivity and translating group-level transcriptional correlates to individual-level genetic risk scores. Moreover, given that the NbM dysconnectivity transcriptional correlates contribute to the early change of Aβ42/40 biomarkers, our findings could offer new insights into the early pathological mechanisms and accelerate future clinical early interventions of Alzheimer's disease.

Availability of data and materials

ADNI neuroimaging and genomic data are publicly available at https://ida.loni.usc.edu. Genomic data for 1000 Genomics Project can be downloaded from https://ftp-trace.ncbi.nih.gov/1000genomes/ftp/release/20130502/. GTEx tissue specific gene expression and eQTL data are shared at https://gtexportal.org/home/datasets. Microarray datasets from six donors are hosted at https://human.brain-map.org/static/download. Also, the MSBB study microarray datasets of 19 brain regions as part of the AMP-Alzheimer's disease project can be accessed at https://www.synapse.org/#!Synapse:syn16809559.

Fundings

This work was supported by the National Natural Science Foundation of China (Nos. 62032007 and 61822108 to Q.J., Nos. 82072000 and 81671769 to L.X.), the Fundamental Research Funds for the Central Universities of China (Grant No. HIT. NSRIF. 2020042 to L.X.), the Natural Science Foundation of Heilongjiang Province, China (Grant No. LH2019H001 to L.X.).

CRediT authorship contribution statement

Peng Ren: Conceptualization, Methodology, Software, Writing – original draft. **Wencai Ding:** Conceptualization, Methodology, Software, Writing – original draft. **Siyang Li:** Data curation, Methodology. **Guiyou Liu:** Data curation, Methodology. **Meng Luo:** Data curation, Methodology. **Wenyang Zhou:** Writing – original draft. **Rui Cheng:** Writing – original draft. **Yiqun Li:** Data curation, Methodology. **Pingping Wang:** Investigation, Validation, Visualization. **Zhipeng Li:** Investigation, Validation, Visualization. **Lifen Yao:** Investigation, Validation, Visualization. **Qinghua Jiang:** Conceptualization, Methodology, Investigation, Supervision, Writing – review & editing. **Xia Liang:** Conceptualization, Methodology, Investigation, Supervision, Writing – review & editing.

Declaration of Competing Interest

All authors report no competing interests except the Alzheimer's Disease Neuroimaging Initiative:

Dr. Petersen serves on scientific advisory boards for Elan Corporation, Wyeth, and GE Healthcare; receives royalties from the publication of Mild Cognitive Impairment (Oxford University Press, 2003); and receives research support from the NIH/NIA (U01 AG06786 [PI], P50 AG16574 [PI], U01 AG 024904 [Subcontract PI], and R01 AG11378 [Co-I]). Dr. Aisen serves on a scientific advisory board for NeuroPhage; serves as a consultant to Elan Corporation, Wyeth, Eisai Inc., Neurochem Inc., Schering-Plough Corp., Bristol-Myers Squibb, Eli Lilly and Company, NeuroPhage, Merck & Co., Roche, Amgen, Genentech, Inc., Abbott, Pfizer Inc, Novartis, and Medivation, Inc.; receives research support from Pfizer Inc, Baxter International Inc., Neuro-Hitech, Abbott, Martek, and the NIH (NIA U01-AG10483 [PI], NIA U01-AG024904 [Coordinating Center Director], NIA R01-AG030048 [PI], and R01-AG16381 [Co-I]); and has received stock options from Medivation, Inc. and NeuroPhage. Dr. Beckett received funding for travel to attend a conference not funded by industry; and receives research support from the NIH (2 P30 AG10129 [Director of Biostatistics Core], 2 P30 CA93373 [Director of Biostatistics Shared Resource], 1 U01 AG24904 [PI, UC Davis site; Biostatistics Team Leader], 1KL2RR024144-01 [Director of Biostatistics Core], 5R01EB002138-07 [Co-I], and 1RC2AG036535-01 [PI, UC Davis site]). Dr. Donohue receives research support from the NIH (AG010483 [Statistician] and AG024904 [Statistician]), the General Clinical Research Center, UCSD, National Center for Research Resources, and from the United States Public Health Service. Dr. Gamst served on an expert review board for Neurochem Inc; and receives research support as an investigator from the NIH [MH22005, CA104573, AG024904, MH062512, DK075128, AG010483, MH079752AG031224, MH083552, MH083506, HL095089], and the National Science Foundation. Dr. Harvey serves as an Associate Editor of Statistics for Alzheimer Disease and Associated Disorders; and receives research support from the NIH (NIA 2P30AG10129 [Biostatistician], NIA R01AG029672 [Biostatistician], NIA 1U01AG24904 [Member of Biostatistics Core], NRCC RL1NS062412 [Biostatistician], NIA R01AG031252 [Biostatistician], 1RC2AG036535– 01 [Member of Biostatistics Team]) and from the Hillblom Foundation, 2007A005NET (Biostatistician). Dr. Jack served on a scientific advisory board for Elan Corporation; receives research support from Pfizer Inc, the NIH (NIA AG11378 [PI], P50-AG16574 [Co-I], and U01 AG024904 [Co-I]) and from the Mayo U of MN Biotechnology Partnership; and holds stock in GE Healthcare. Dr. Jagust has served on a scientific advisory boards for Genentech, Inc.; has served as a consultant for Synarc, Elan Corporation, Genentech, Inc., Ceregene, Schering Plough, and Merck & Co; and receives research support from the NIH (AG027859 [PI], AG027984 [PI], and AG 024904 [Co-I]) and from the Alzheimer's Association. Dr. Shaw has received funding for travel and speaker honoraria from Pfizer Inc; serves on the editorial board of Therapeutic Drug Monitoring; may potentially receive revenue for patent pending (application 10/192,193): *O*-methylated rapamycin derivatives for alleviation and inhibition of lymphoproliferative disorders, licensed by the University of Pennsylvania to Novartis; receives royalties from publication of Applied Pharmacokinetics and Pharmacodynamics: Principles of Therapeutic Drug Monitoring, Wolters Kluwer/Lippincott Williams & Wilkins, 2005; receives research support from the NIH (AG024904 [Co-PI Biomarker Core Laboratory]); and receives board of directors' compensation and holds stock options in Saladax Biomedical. Dr. Toga received a speaker

honorarium from St. Jude Children's Hospital; serves in an editorial capacity for NeuroImage, InSight, The Cerebellum, Neuroimaging, Neuroinformatics, Anatomy & Embryology, Current Medical Imaging Reviews, Biology Image Library, Biomedical Computation Review, Brain Structure and Function, and Journal of Neural Regeneration Research; has served on scientific and/or external advisory boards for Wellcome Trust, Allen Institute for Brain Science, University of Texas at Austin, Oklahoma IDeA Network for Biomedical Research Excellence, Takeda Global Research & Development Center, and the University of Pittsburgh; and has received/receives research support from the NIH (1R01 HD053893-01 [Co-I], NIBIB 2 R01 LM005639 [Co-I], NCRR 5 P41 RR013642 [PI], R01 HD050735-01 [Co-I], 1 R01 NS049194 [Co-I], 1 R01 EB 006266-01 [Subcontract PI], NIMH/UCI, R24 RR021992 [Subcontract PI], 2P50AG005133 [Consultant: Core-Neuroimaging], NCRR 5 U24 RR021760 [PI], NIMH 2 P50 AG016570 [Co-I], NIMH 1R01MH072641-01A1 [Co-I], NIMH 5 R01 MH071940 [PI], NIMH/NIA 1 U01 AG024904 [Subcontract PI], NIMH/MGH, R24 RR021382 [Subcontract PI], NIBIB/BWH 1 U54 EB05149 [Subcontract PI], 1 R01 DA017830 [Co-I], NCRR 5 U54 RR021813 [PI], R01 MH069259 [Subcontract PI], 1 R01 NS050792 [Subcontract PI], MH069433 [Co-I], NIMH 9 P01 EB 001955-11 [CoPI]), 2005 Equipment Grant, and an Academic Excellence Grant–SUN Microsystems, and from High-Q Foundation and the National Multiple Sclerosis Society. Dr. Trojanowski has received funding for travel and honoraria from Takeda Pharmaceutical Company Ltd. and to attend numerous conferences not funded by industry; serves as an Associate Editor of Alzheimer's & Dementia; holds 14 patents that may accrue revenue: US Patent 5,281,521, issued 25 Jan 1994: Modified Avidin-Biotin Technique; US Patent 5,580,898, issued 3 Dec 1996: Method of Stabilizing Microtubules to Treat Alzheimer's Disease; US Patent 5,601,985, issued 11 Feb 1997: Method of Detecting Abnormally Phosphorylated Tau; US Patent 5,733,734, issued 31 Mar 1998: Method of Screening for Alzheimer's Disease or Disease Associated with the Accumulation of Paired Helical Filaments; US Patent 5,792,900, issued 11 Aug 1998: Compositions and Methods for Producing and Using Homogeneous Neuronal Cell Transplants; US Patent 5,849,988, issued 15 Dec 1998: Rat Comprising Straight Filaments in Its Brain; US Patent 6,214,334, issued 10 Apr 2001: Compositions And Methods for Producing and Using Homogeneous Neuronal Cell Transplants to Treat Neurodegenerative Disorders and Brain and Spinal Cord Injuries; US Patent 6,358,681, issued 19 Mar 2002: Diagnostic Methods for Alzheimer's Disease by Detection of Multiple MRNAs; US Patent 6,727,075, issued 27 Mar 2004: Methods and Compositions for Determining Lipid Peroxidation Levels in OxidantStress Syndromes and Diseases; US Patent 7,011,827, issued 14 Mar 2006: Compositions and Methods for Producing and Using Homogenous Neuronal Cell Transplants; Penn 0652, K1828, filed 5 Aug 1998: Method of Identifying, Diagnosing and Treating Alpha-synuclein Positive Neurodegenerative Disorders; Penn L1986, Filed 13 Nov 1998: Mutation-specific Functional Impairments in Distinct Tau Isoforms of Hereditary Frontotemporal Dementia and Parkinsonism Linked to Chromosome-17: Genotype Predicts Phenotype; Penn R3868 (UPN-4439), filed 28 Feb 2005: Microtubule Stabilizing Therapies for Neurodegenerative Disorders; and Penn S-4018, DB&R 46406-217282, filed 22 Nov 2005: Treatment of Alzheimer's and Related Diseases with an Antibody; and receives research support from the NIH (NIA P01 AG 09215-20 [PI], NIA P30 AG 10124-18 [PI], NIA PO1 AG 17586-10 [Project 4 Leader], NIA 1PO1 AG-19724-07 [Core C Leader], NIA 1 U01 AG 024904-05 [Co-PI Biomarker Core Laboratory], NINDS P50 NS053488-02 [PI], NIA UO1 AG029213-01 [Co-I]; RC2NS069368 [PI], RC1AG035427 [PI], and NIA P30AG036468 [PI]), and from the Marian S. Ware Alzheimer Program. Dr. Weiner serves on scientific advisory boards for Bayer Schering Pharma, Eli Lilly and Company, CoMentis, Inc., Neurochem Inc, Eisai Inc., Avid Radiopharmaceuticals Inc., Aegis Therapies, Genentech, Inc., Allergan, Inc., Lippincott Williams & Wilkins, Bristol-Myers Squibb, Forest Laboratories, Inc., Pfizer Inc, McKinsey & Company, Mitsubishi Tanabe Pharma Corporation, and Novartis; has received funding for travel from Nestle´and Kenes International and to attend conferences not funded by industry; serves on the editorial board of Alzheimer's & Dementia; has received honoraria from the Rotman Research Institute and BOLT International; serves as a consultant for Elan Corporation; receives research support from Merck & Co., Radiopharmaceuticals Inc., the NIH (U01AG024904 [PI], P41 RR023953 [PI], R01 AG10897 [PI], P01AG19724 [Co-I], P50AG23501 [Co-I], R24 RR021992 [Co-I], R01 NS031966 [Co-I], and P01AG012435 [Co-I]), the US Department of Defense (DAMD17- 01-1-0764 [PI]), the Veterans Administration (MIRECC VISN 21 [Core PI]), and from the State of California; and holds stock in Synarc and Elan Corporation.

Data availability

data availability has been specified

Acknowledgements

Data collection and sharing for this project was funded by the Alzheimer's Disease Neuroimaging Initiative (ADNI) (National Institutes of Health Grant U01 AG024904) and DOD ADNI (Department of Defense award number W81XWH-12-2-0012). ADNI is funded by the National Institute on Aging, the National Institute of Biomedical Imaging and Bioengineering, and through generous contributions from the following: AbbVie, Alzheimer's Association; Alzheimer's Drug Discovery Foundation; Araclon Biotech; BioClinica, Inc.; Biogen; Bristol-Myers Squibb Company; CereSpir, Inc.; Cogstate; Eisai Inc.; Elan Pharmaceuticals, Inc.; Eli Lilly and Company; EuroImmun; F. Hoffmann-La Roche Ltd. and its affiliated company Genentech, Inc.; Fujirebio; GE Healthcare; IXICO Ltd.; Janssen Alzheimer Immunotherapy Research & Development, LLC.; Johnson & Johnson Pharmaceutical Research & Development LLC.; Lumosity; Lundbeck; Merck & Co., Inc.; Meso Scale Diagnostics, LLC.; NeuroRx Research; Neurotrack Technologies; Novartis Pharmaceuticals Corporation; Pfizer Inc.; Piramal Imaging; Servier; Takeda Pharmaceutical Company; and Transition Therapeutics. The Canadian Institutes of Health Research is providing funds to support ADNI clinical sites in Canada. Private sector contributions are facilitated by the Foundation for the National Institutes of Health (www.fnih.org). The grantee organization is the Northern California Institute for Research and Education, and the study is coordinated by the Alzheimer's Therapeutic Research Institute at the University of Southern California. ADNI data are disseminated by the Laboratory for Neuro Imaging at the University of Southern California. The Genotype-Tissue Expression (GTEx) Project was supported by the Common Fund of the Office of the Director of the National Institutes of Health, and by NCI, NHGRI, NHLBI, NIDA, NIMH, and NINDS. The results published here are in whole or in part based on data obtained from the AD Knowledge Portal (https://adknowledgeportal.org/). These data were generated from postmortem brain tissue collected through the Mount Sinai VA Medical Center Brain Bank and were provided by Dr. Eric Schadt from Mount Sinai School of Medicine. We also would like to thank Editage (www.editage.cn) for English language editing.

Appendix A. Supplementary data

Supplementary data to this article can be found online at https://doi.org/10.1016/j.nbd.2022.105983.

References

Altshuler, D.M., et al., 2015. A global reference for human genetic variation. Nature. 526, 68.

Arnatkeviciute, A., et al., 2019. A practical guide to linking brain-wide gene expression and neuroimaging data. Neuroimage. 189, 353–367.

Asleh, J., et al., 2020. Brain-wide structural and functional disruption in mice with oligodendrocyte-specific Nf1 deletion is rescued by inhibition of nitric oxide synthase. Proc. Natl. Acad. Sci. U. S. A. 117, 22506–22513.

Desikan, R.S., et al., 2017. Genetic assessment of age-associated Alzheimer disease risk: development and validation of a polygenic hazard score. PLoS Med. 14, e1002258.
Do, J.P., et al., 2016. Cell type-specific long-range connections of basal forebrain circuit. Elife. 5, e13214.
Dong, Q.Y., et al., 2021. Glucose metabolism in the right middle temporal gyrus could be a potential biomarker for subjective cognitive decline: a study of a Han population. Alzheimers Res. Ther. 13, 74.
Eickhoff, S.B., et al., 2005. A new SPM toolbox for combining probabilistic cytoarchitectonic maps and functional imaging data. Neuroimage. 25, 1325–1335.
Fernandez-Cabello, S., et al., 2020. Basal forebrain volume reliably predicts the cortical spread of Alzheimer's degeneraion. Brain. 143, 993–1009.
Fields, R.D., et al., 2015. Glial regulation of the neuronal connectome through local and long-distant communication. Neuron. 86, 374–386.
Grilli, M., et al., 2009. Nicotinic and muscarinic cholinergic receptors coexist on GABAergic nerve endings in the mouse striatum and interact in modulating GABA release. Neuropharmacology. 56, 610–614.
Grothe, M., et al., 2013. Longitudinal measures of cholinergic forebrain atrophy in the transition from healthy aging to Alzheimer's disease. Neurobiol. Aging 34, 1210–1220.
Guo, J.-D., et al., 2012. Presynaptic muscarinic M2 receptors modulate glutamatergic transmission in the bed nucleus of the stria terminalis. Neuropharmacology. 62, 1671–1683.
Haroutunian, V., et al., 2009. Transcriptional vulnerability of brain regions in Alzheimer's disease and dementia. Neurobiol. Aging 30, 561–573.
Hawrylycz, M.J., et al., 2012. An anatomically comprehensive atlas of the adult human brain transcriptome. Nature. 489, 391–399.
Hawrylycz, M., et al., 2015. Canonical genetic signatures of the adult human brain. Nat. Neurosci. 18, 1832–1844.
Herdick, M., et al., 2020. Multimodal MRI analysis of basal forebrain structure and function across the Alzheimer's disease spectrum. Neuroimage-Clinical. 28, 102495.
Hodes, R.J., Buckholtz, N., 2016. Accelerating medicines partnership: Alzheimer's disease (AMP-AD) knowledge portal aids Alzheimer's drug discovery through open data sharing. Expert Opin. Ther. Targets 20, 389–391.
Kanehisa, M., Goto, S., 2000. KEGG: Kyoto encyclopedia of genes and genomes. Nucleic Acids Res. 28, 27–30.
Kawamura, A., et al., 2020. Chd8 mutation in oligodendrocytes alters microstructure and functional connectivity in the mouse brain. Mol. Brain. 13, 1–15.
Kerbler, G.M., et al., 2015. Basal forebrain atrophy correlates with amyloid β burden in Alzheimer's disease. NeuroImage: Clinical. 7, 105–113.
Lehner, K.R., et al., 2019. Forebrain cholinergic signaling regulates innate immune responses and inflammation. Front. Immunol. 10, 585.
Li, H., et al., 2017. Altered functional connectivity of the basal nucleus of Meynert in mild cognitive impairment: a resting-state fMRI study. Front. Aging Neurosci. 9, 127.
Liang, X., et al., 2013. Coupling of functional connectivity and regional cerebral blood flow reveals a physiological basis for network hubs of the human brain. Proc. Natl. Acad. Sci. U. S. A. 110, 1929–1934.
Lu, H., et al., 2019. Origins of the resting-state functional MRI signal: potential limitations of the "Neurocentric" model. Front. Neurosci. 13, 1136.
Luo, W.J., et al., 2009. GAGE: generally applicable gene set enrichment for pathway analysis. Bmc Bioinform. 10, 161.
Marchitelli, R., et al., 2018. Simultaneous resting-state FDG-PET/fMRI in Alzheimer disease: relationship between glucose metabolism and intrinsic activity. Neuroimage. 176, 246–258.
Marees, A.T., et al., 2018. A tutorial on conducting genome-wide association studies: quality control and statistical analysis. Int. J. Methods Psychiatr. Res. 27, e1608.
Marigorta, U.M., et al., 2017. Transcriptional risk scores link GWAS to eQTLs and predict complications in Crohn's disease. Nat. Genet. 49, 1517.
Meng, D., et al., 2018. Altered nucleus basalis connectivity predicts treatment response in mild cognitive impairment. Radiology. 289, 775–785.
Meng, Y., et al., 2019. Resting state functional connectivity changes after MR-guided focused ultrasound mediated blood-brain barrier opening in patients with Alzheimer's disease. Neuroimage. 200, 275–280.
Moon, H.S., et al., 2021. Contribution of excitatory and inhibitory neuronal activity to BOLD fMRI. Cereb. Cortex 31, 4053–4067.
Nizari, S., et al., 2021. Loss of cholinergic innervation differentially affects eNOS-mediated blood flow, drainage of a beta and cerebral amyloid angiopathy in the cortex and hippocampus of adult mice. Acta Neuropathol. Commun. 9, 12.
Pa, J., et al., 2013. Cholinergic enhancement of functional networks in older adults with mild cognitive impairment. Ann. Neurol. 73, 762–773.
Qi, J., et al., 2021. Altered functional connectivity between the nucleus basalis of Meynert and anterior cingulate cortex is associated with declined attentional performance after total sleep deprivation. Behav. Brain Res. 409, 113321.
Roher, A.E., et al., 2000. Cortical cholinergic denervation elicits vascular a beta deposition. Vasc. Factors Alzheimer's Dis. 903, 366–373.
Román, G.C., Kalaria, R.N., 2006. Vascular determinants of cholinergic deficits in Alzheimer disease and vascular dementia. Neurobiol. Aging 27, 1769–1785.
Santangelo, R., et al., 2020. CSF p-tau/Aβ42 ratio and brain FDG-PET may reliably detect MCI "imminent" converters to AD. Eur. J. Nucl. Med. Mol. Imaging 47, 3152–3164.
Schliebs, R., Arendt, T., 2011. The cholinergic system in aging and neuronal degeneration. Behav. Brain Res. 221, 555–563.
Schmitz, T.W., et al., 2016. Basal forebrain degeneration precedes and predicts the cortical spread of Alzheimer's pathology. Nat. Commun. 7, 13249.
Schmitz, T.W., et al., 2018. Longitudinal Alzheimer's degeneration reflects the spatial topography of cholinergic basal forebrain projections. Cell Rep. 24, 38–46.
Schmitz, T.W., et al., 2020. Longitudinal basal forebrain degeneration interacts with TREM2/C3 biomarkers of inflammation in presymptomatic Alzheimer's disease. J. Neurosci. 40, 1931–1942.
Seidlitz, J., et al., 2020. Transcriptomic and cellular decoding of regional brain vulnerability to neurogenetic disorders. Nat. Commun. 11, 3358.
Sjöstedt, E., et al., 2020. An atlas of the protein-coding genes in the human, pig, and mouse brain. Science. 367, eaay5947.
Subramanian, A., et al., 2005. Gene set enrichment analysis: a knowledge-based approach for interpreting genome-wide expression profiles. Proc. Natl. Acad. Sci. U. S. A. 102, 15545–15550.
Teipel, S., et al., 2014. Cholinergic basal forebrain atrophy predicts amyloid burden in Alzheimer's disease. Neurobiol. Aging 35, 482–491.
Wang, M.H., et al., 2016. Integrative network analysis of nineteen brain regions identifies molecular signatures and networks underlying selective regional vulnerability to Alzheimer's disease. Genome Med. 8, 104.
Wang, T., et al., 2019. Polygenic risk score for Alzheimer's disease is associated with Ch4 volume in normal subjects. Front. Genet. 10.
Weigand, A.J., et al., 2020. Association of anticholinergic medications and AD biomarkers with incidence of MCI among cognitively normal older adults. Neurology. 95, e2295–e2304.
Wightman, D.P., et al., 2021. A genome-wide association study with 1,126,563 individuals identifies new risk loci for Alzheimer's disease. Nat. Genet. 53, 1276–1282.
Witten, I.B., et al., 2010. Cholinergic interneurons control local circuit activity and cocaine conditioning. Science. 330, 1677–1681.
Woolf, N.J., 1991. Cholinergic systems in mammalian brain and spinal-cord. Prog. Neurobiol. 37, 475–524.
Xu, H., et al., 2021. Long-term effects of cholinesterase inhibitors on cognitive decline and mortality. Neurology. 96, e2220–e2230.
Zaborszky, L., et al., 2008. Stereotaxic probabilistic maps of the magnocellular cell groups in human basal forebrain. Neuroimage. 42, 1127–1141.
Zhou, X.P., et al., 2021. Polygenic score models for Alzheimer's disease: from research to clinical applications. Front. Neurosci. 15, 650220.